Materials & Design 206 (2021) 109824

Contents lists available at ScienceDirect

Materials & Design

journal homepage: www.elsevier.com/locate/matdes

Design of Fe-containing GdTbCoAl high-entropy-metallic-glass composite microwires with tunable Curie temperatures and enhanced cooling efficiency

Hangboce Yin [a,b], Jiayan Law [b], Yongjiang Huang [a,*], Victorino Franco [b], Hongxian Shen [a,*], Sida Jiang [c,*], Ying Bao [a], Jianfei Sun [a]

[a] School of Materials Science and Engineering, Harbin Institute of Technology, Harbin 150001, China
[b] Dpto. Física de la Materia Condensada, ICMS-CSIC, Universidad de Sevilla, Sevilla 41080, Spain
[c] Space Environment Simulation Research Infrastructure, Harbin Institute of Technology, Harbin 150001, China

HIGHLIGHTS

- Nanocrystalline Fe-containing GdTbCoAl high-entropy-metallic-glass were attained.
- Curie temperature is tuned by Fe-doping in a wide temperature range of 81–108 K.
- Magnetic entropy change 7.6–8.9 J kg^{-1} K^{-1} for 5 T were achieved.
- The dual-phase structure with T_C distribution enhances the cooling efficiency.

GRAPHICAL ABSTRACT

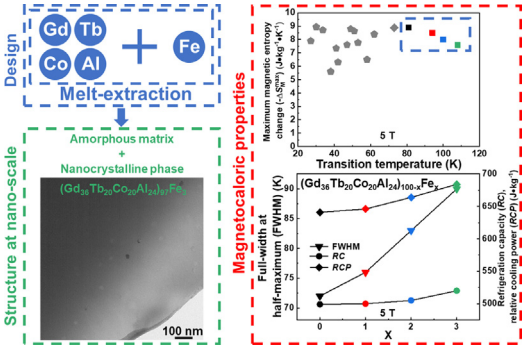

ARTICLE INFO

Article history:
Received 26 January 2021
Revised 6 May 2021
Accepted 10 May 2021
Available online 12 May 2021

Keywords:
Fe-doping
Dual-phase microstructure
Cooling efficiency
Microwires
Magnetocaloric effect

ABSTRACT

Through designing the composition and processing approach, the non-equiatomic $(Gd_{36}Tb_{20}Co_{20}Al_{24})_{100-x}Fe_x$ (x = 0, 1, 2 and 3 at.%) high-entropy-metallic-glass (HE-MG) alloy microwires were successfully fabricated by melt-extraction technique. The microstructure and magnetocaloric properties of the microwires were systematically investigated. The microwires possess tunable Curie temperatures, i.e. 81–108 K, above the typical rare-earth (RE) containing HE-MG reports. The high Curie temperatures are attributed to the designed composition. Magnetocaloric response peak values of Fe-containing GdTbCoAl alloy microwires range 7.6–8.9 J kg^{-1} K^{-1} (5 T), which are comparable to those of many outstanding RE-containing magnetocaloric HE-MGs. The characteristics of the melt-extraction method, combining with compositional effects, favor the formation of amorphous and nanocrystalline phases. The increase in the cooling efficiency for microwires with higher Fe content can be attributed to the broadening of the Curie temperature distribution induced by the composition difference between nanocrystalline phase and amorphous matrix. The designed composition and the melt-extraction processing approach for Fe-containing GdTbCoAl alloys can tune their Curie temperatures towards a temperature range of natural gas liquefaction and improve their magnetocaloric properties. This demonstrates that Fe-containing GdTbCoAl HE-MG composite microwires have great potential as high-performance magnetic refrigerants.

* Corresponding authors.
E-mail addresses: yjhuang@hit.edu.cn (Y. Huang), hitshenhongxian@163.com (H. Shen), jiangsida@hit.edu.cn (S. Jiang).

https://doi.org/10.1016/j.matdes.2021.109824
0264-1275/

1. Introduction

Magnetic refrigeration based on the magnetocaloric effect (MCE) of solid state materials has been widely considered as a promising candidate for the conventional gas compression-expansion refrigeration, due to its excellent cooling efficiency and environmental friendliness [1]. Magnetocaloric materials (MCMs) exploit the adiabatic temperature change when subjected to an applied varying magnetic field where they can act as solid refrigerants. The MCE property can be characterized by the magnetic entropy change ($-\Delta S_M$).

Typically, the MCE performance can be optimized by two ways, i.e., i) compositional design and ii) design of processing approach. With an appropriate compositional design, desired phase selection could optimize MCE performance and aid the T_C tunability. As an example, MCMs with amorphous and nanocrystalline phases have been reported showing enhanced cooling efficiency with appropriately large maximum magnetic entropy change ($-\Delta S_M^{max}$) in an extended temperature range [2,3]. These characteristics have great potential for Ericsson cycle refrigeration [4]. For the second approach to optimize MCE performance, it has been reported that MCMs with reduced dimensions could facilitate the design of magnetic refrigerators, especially in heat transferability [5–7]. In particular, MCMs processed into wire forms show great suitability among other reduced dimensions (such as laminar or particles) due to its high surface-to-volume ratio, superior mechanical stability, large degree of packing, great temperature span between ends, and high pressure drop [7,8]. Using the melt-extraction technique, high quality metallic microwires (micro-size diameters) can be easily obtained. As the MCM wire dimensions reduce to micro-sized diameters, it can further foster an increase in the cooling load, cooling efficiency of the system and pressure drop of the MCMs [7]. This indicates that it is of great significance to study MCM microwires as this form can greatly facilitate the design of magnetocaloric refrigerators. In addition, amorphous/nanocrystalline dual-phase structure could be developed in melt-extracted microwires without additional post heat treatment. This is facilitated by the great cooling rate difference between the region in contact with the wheel and the free surface of the melt during the melt-extraction process, which has been proven by the previous work of our group [9,10].

High-entropy-alloys (HEAs), as a highly regarded new class of materials, are designed with multiple principal alloying elements to yield high configurational entropy, unlike the traditional materials whose designs are based on one or two main elements. Since HEAs were firstly reported in 2004 [11,12], they have evolved from the first-generation quinary equimolar single-phase families to the second-generation HEAs, extending compositions to four or more principal components in non-molar concentrations and/or with multi-phases [13]. MCE HEAs mainly focus on rare-earth (RE) containing high-entropy-metallic-glasses (HE-MGs), which possess extremely low magnetic hysteresis and excellent MCE properties [14–17]. Analogous to HEAs, MCE RE-containing HE-MGs also report an evolution trend of first → second generation compositions, starting with equiatomic compositions (e.g. GdTbDyAl(Fe/Co/Ni) [16], HoErCoAl(Gd/Dy/Tm) [17]) to non-equiatomic compositions (e.g. $Gd_{36}Y_{20}Co_{20}Al_{24}$ [15]). However, both generations tend to exhibit low transition temperatures, mainly ranging <60 K where they exhibit $-\Delta S_M^{max}$ values, typical of the MCE characteristics. Hence, MCE RE-containing HE-MGs are still at an emerging stage and it is essential to optimize them with tunable transition temperatures, like Curie temperatures (T_C), and extend to higher temperature range for this new class of magnetocaloric alloys.

Xue et al. [14] designed the quaternary equimolar GdHoCoAl and GdTbCoAl HE-MGs and found that T_C can be greatly tuned from 50 K to 73 K when substituting to Tb. In addition, the equimolar GdTbCoAl HE-MG possesses outstanding MCE performance: $-\Delta S_M^{max}$ of 8.88 J kg^{-1} K^{-1} and relative cooling power (*RCP*) of 577 J kg^{-1} for $\mu_0\Delta H$ = 5 T. One possible way to further optimize MCE RE-containing HE-MGs for higher temperature range is Fe-doping, which has been reported to effectively increase T_C and improve the MCE properties of Gd-based metallic glasses [18–20]. Furthermore, the heat of mixing (ΔH_{AB}^{mix}), which can affect the type of phase formation, is found to be negative although small for atom pairs between Fe and RE/transition elements: −1, −3 and −1 kJ mol^{-1} for Fe-Gd, Fe-Tb and Fe-Co, respectively [21]. Large negative ΔH_{AB}^{mix}values between the dopant and main elements would favor the glass forming ability (GFA) [9,22,23]. Therefore, the resultant small values of ΔH_{AB}^{mix} indicate that designing compositions of GdTbCoAl with Fe-doping could enable the formation of dual-phase microstructure consisting of amorphous and nanocrystalline phases.

Hence, the purpose of this paper is to design and prepare RE-containing HE-MG composite microwires with widely tunable T_C above the typical limit (<60 K), with amorphous and nanocrystalline phases and enhanced MCE properties. For that, we selected the compositional design which is fulfilled as the second-generation MCE RE-containing HE-MG with minor Fe additions: $(Gd_{36}Tb_{20}Co_{20}Al_{24})_{100-x}Fe_x$ where x = 0 to 3 at.%. These alloys were processed into microwires with structure evolution from single phase (amorphous phase) to two phases (amorphous and nanocrystalline phases), which show tunable T_C from 81 to 100 K with relatively large MCE properties. The successful MCE optimization of these microwires demonstrate that appropriate compositional design and processing technique can pave a new pathway to design and fabricate high-performance MCMs as well as for the HEA community.

2. Experimental methods

The master alloys with nominal compositions of $(Gd_{36}Tb_{20}Co_{20}Al_{24})_{100-x}Fe_x$ (x = 0, 1, 2 and 3 at.%) were firstly fabricated by arc-melting a mixture of constituent elements (each with purity higher than 99.9 wt%) under a Ti-gettered high-purity Ar atmosphere. According to the Fe addition contents, samples studied in this work are denoted hereafter as Fe0, Fe1, Fe2 and Fe3. The alloy ingots were re-melted at least five times to ensure chemical homogeneity, followed by suction casting into a copper mold to form cylindrical rods with 10 mm in diameter and 50 mm in length. Subsequently, the alloy microwires were prepared by using a melt-extraction facility with a molybdenum (Mo) wheel. The line speed of Mo wheel was 30 m s^{-1}. The melt-extraction process was under an Ar atmosphere. For alloys with Fe content higher than 3 at.%, e.g. 4 and 5 at.%, their microwires could not be prepared within the limits of the melt-extraction equipment. The details can be found in Supplementary Information Document and Fig. S1.

The surface morphology of the microwires was examined by a scanning electron microscope (SEM, FEI Quanta 200FEG). Fig. 1(a) shows the smooth surface of the Fe3 microwires. The macroscopic view and the cross-sectional SEM image of Fe3 microwires are shown in Fig. S2. The cross-sectional SEM image shows that the diameter of Fe3 microwire is ~30 μm. The thermal stability of the samples was studied by differential scanning calorimeter (DSC, Netzsch STA449F3 Jupiter) at a heating rate of 10 K min^{-1}. The microstructure and compositional information were examined by transmission electron microscope (TEM, FEI Talos F200X) equipped with energy-dispersive X-ray spectroscopy (EDS). Temperature dependence of magnetization (M–T) and magnetic field dependence of magnetization (M–H) were measured by using a Physical Property Measurement System (PPMS, Quantum Design Dynacool-14 T). For a large signal to noise ratio, a bundle of micro-

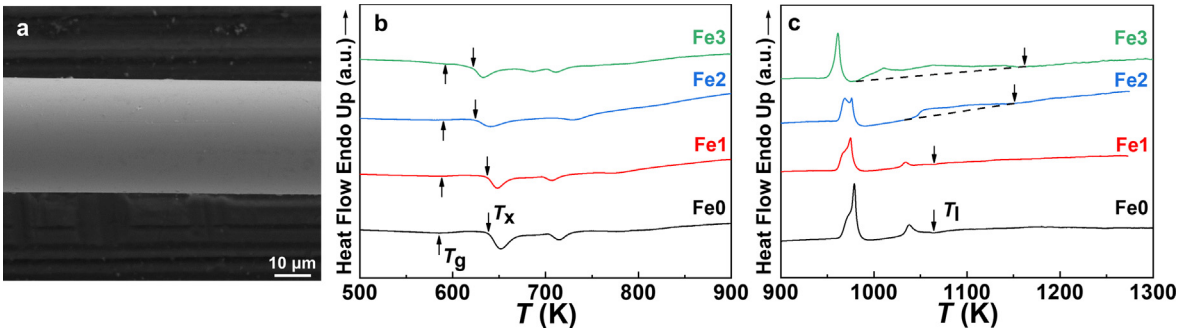

Fig. 1. (a) SEM image of the Fe3 microwire, (b) and (c) DSC results of the Fe0, Fe1, Fe2 and Fe3 microwires.

wires were used for the magnetic measurements. The microwires were arranged parallel to each other in a non-magnetic polymeric tubular sample holder with 1 mm in inner diameter, 2.5 mm in outer diameter, and 3 mm in length.

3. Results and discussion

DSC curves of Fe0, Fe1, Fe2, and Fe3 microwires are presented in Fig. 1(b) and (c). These curves show the thermophysical parameters including the glass transition temperatures (T_g), the onset temperature of the first crystallization peak (T_x), and the liquidus temperatures (T_l). It is observed that with increasing Fe content, T_g and T_l increase whereas T_x decreases. Their detailed information is summarized in Table 1, together with the super-cooled liquid region ($\Delta T_x = T_x - T_g$) and $\gamma = T_x/(T_g + T_l)$. ΔT_x and γ indicate the thermal stability, i.e. resistance to crystallization [24,25], and the GFA [26] of the supercooled liquid, respectively. As seen in Table 1, the values of ΔT_x and γ monotonically decrease with increasing Fe content, facilitating the precipitation of crystallites on microwires. It should be noted that the largest decrease of ΔT_x and γ takes place between Fe1 and Fe2, suggesting the possibility of microstructural change between these samples. The GFA is affected by these parameters: atomic size difference (δ), the mixing enthalpy (ΔH_{mix}) and the mixing entropy (ΔS_{mix}). These are also widely used to predict the phase formation in HEAs, including HE-MGs [23,27–29]. Hence, these parameters for Fe0, Fe1, Fe2 and Fe3 microwires are calculated and listed in Table 1. For all the studied microwires, these parameters are in agreement to the criteria reported for HE-MG ($\delta \geq 9$, $-49 \leq \Delta H_{mix} \leq -5.5$ kJ mol^{-1} and $7 \leq \Delta S_{mix} \leq 16$ J K^{-1} mol^{-1}) [23]. The authors [23] further report that the formation of amorphous phase is favored by larger δ, smaller ΔS_{mix} and more negative ΔH_{mix} values in comparison with solid solution phases. In our case, δ values evolve very slightly with increasing Fe content, while the changes of ΔS_{mix} and ΔH_{mix} are relatively large. The relatively small effect of Fe-doping on δ is of little help to the atomic packing density, which does not aid the enhancement of GFA. The evolutions of ΔS_{mix} and ΔH_{mix} are in agreement to that of γ. Therefore, the deterioration of the GFA should be ascribed to the relatively large change of ΔH_{mix} and ΔS_{mix} induced by Fe-doping.

TEM observations were performed in order to investigate the microstructures of Fe-containing GdTbCoAl microwires at the nano-scale. The homogeneous maze-like patterns of the high-resolution TEM (HRTEM) images in Fig. 2(a) and (b) indicate the fully amorphous structure of Fe0 and Fe1 microwires, respectively [30]. Their fully amorphous structures are also confirmed by the rather faint and diffused halo rings of the selected area electron diffraction (SAED) patterns without any distinguishable diffraction spot (see insets of Fig. 2(a) and (b)). Fig. 2(c) shows the HRTEM, the corresponding fast Fourier transform (FFT)-inverse fast Fourier transform (IFFT) and SAED images of Fe2 microwire. The FFT-IFFT image with crystalline fringes, corresponding to the red dashed square marked by the number 1, indicates the existence of nanocrystalline phase with a grain size of ~3 nm [31]. The amorphous matrix is confirmed by the bottom-right FFT-IFFT image which shows the completely random atomic arrangement and corresponds to the red dashed square marked by the number 2. As shown in the top-right inset of Fig. 2(c), a light crystalline-ring SAED pattern can be observed besides the strong halo ring corresponding to the amorphous matrix, confirming the dual-phase microstructure. The bright-field TEM image of the surface area of Fe3 microwire is shown in Fig. 2(d). A dual-phase structure can be obviously observed in this image. The presence of the nanocrystals in the amorphous matrix can be confirmed by the corresponding SAED results with the light crystalline diffraction spots and strong halo ring (Fig. 2(e)). The crystalline diffraction spots indicate the nanocrystalline phase is face-centered cubic (FCC) structure. The asymmetric spots can be also observed in the SAED results. To further confirm the structure of the nanocrystalline phase, HRTEM along three different zone axes were obtained, as shown in the top images of Fig. 2(f)–(h). The HRTEM images indicate the nanocrystalline phase with an average grain size of ~27 nm. The FFT images corresponding to the red dashed squares in the HRTEM images confirm FCC structure of the nanocrystalline phase [32], as shown in the bottom images of Fig. 2(f)–(h). Overall, the single amorphous structures of the Fe0 and Fe1 microwires evolve into a dual-phase microstructure with increasing Fe-doping, where nanocrystals are observed (though rather few) for Fe2 and Fe3. This is in line with the evolution of ΔT_x and γ.

For the microwires without Fe-doping, the composition is very close to the ideal glass-forming composition according to Lu's empirical concept [33]. This composition normally means the best glass-forming composition for an alloy. With the increase of Fe

Table 1
The thermophysical parameters of Fe0, Fe1, Fe2 and Fe3 microwires.

Sample	T_g (K)	T_x (K)	T_l (K)	ΔT_x (K)	γ	δ	ΔH_{mix} (kJ mol^{-1})	ΔS_{mix} (J K^{-1} mol^{-1})
Fe0	586	638	1064	52	0.386	14.31	−34.63	11.25
Fe1	588	637	1065	49	0.385	14.44	−34.08	11.61
Fe2	590	624	1155	34	0.357	14.56	−33.53	11.84
Fe3	592	622	1162	30	0.354	14.68	−32.99	12.02

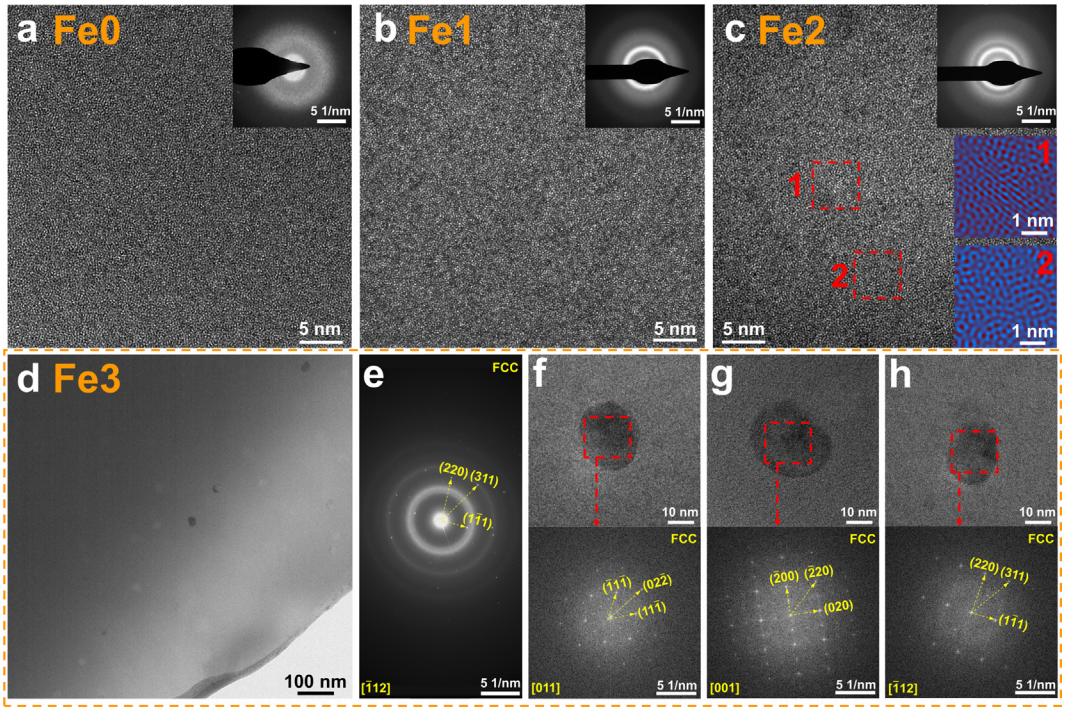

Fig. 2. HRTEM images and corresponding SAED results (insets) of (a) Fe0, (b) Fe1 and (c) Fe2 microwires, respectively. Corresponding FFT-IFFT results of the red dashed squares marked by numbers 1 and 2 are also shown in the insets of (c). (d) and (e) show the bright-field TEM image and the corresponding SAED results of Fe3 microwire, respectively. (f), (g) and (h) show HRTEM images (top) and FFT results (bottom) corresponding to the red dashed squares in HRTEM images of Fe3 microwire along three different zone axes.

content, the thermal stability and GFA of Fe-containing GdTbCoAl microwires deteriorate. During the melt-extraction process, the melt surface can be divided into two regions, i.e., the region in contact with the wheel and the free surface. The cooling rate of the region in contact with the wheel reaches a high value of over 10^6 K s^{-1}, favoring the formation of amorphous phase. Contrarily, for the free surface, the cooling rate is much lower, facilitating the formation of nanocrystals if the GFA of the alloy is not high enough [9,10]. Due to the deteriorated GFA and relatively low cooling rate at the free surface, nanocrystals could be created in the case of Fe-containing GdTbCoAl microwires. Two parameters can favor the growth of nanocrystal in the liquid, i.e. the remarkable long-distance atomic diffusion [34] and the high mobility of atoms [27,35]. In supercooled liquids of Fe-containing GdTbCoAl microwires, the atomic diffusion is kinetically retarded by the high degree of dense random packing, which is attributed to the relatively large absolute values of δ and ΔH_{mix} [34,36,37]. The increased melt viscosity of GdTbCoAlFe liquids, which is induced by Fe-doping [37], kinetically restricts the mobility of the atoms [35,38]. Accordingly, the nanocrystalline phase which exists in the liquid is retained in Fe-containing GdTbCoAl microwires.

Fig. 3 shows the temperature dependence of the field cooling magnetization (M_{FC}) for Fe0, Fe1, Fe2 and Fe3 microwires, measured under a field of 200 Oe. An extrapolation method for the linear part of the M–T curve is used to confirm the $T_{C,}$ which is the

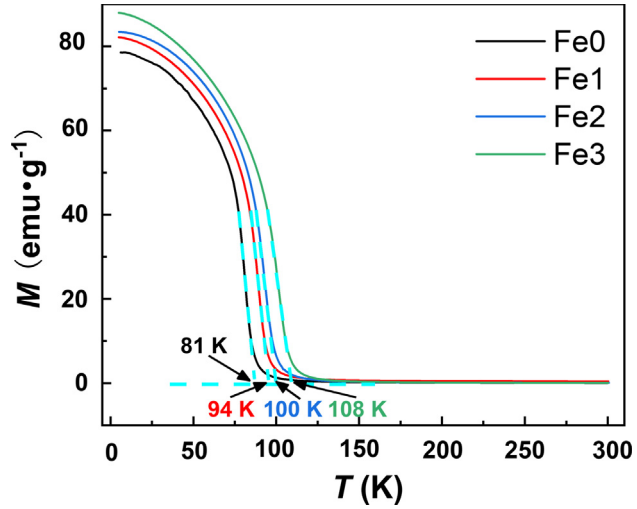

Fig. 3. Temperature dependence of M_{FC} curves for Fe0, Fe1, Fe2 and Fe3 microwires under an applied magnetic field of 200 Oe.

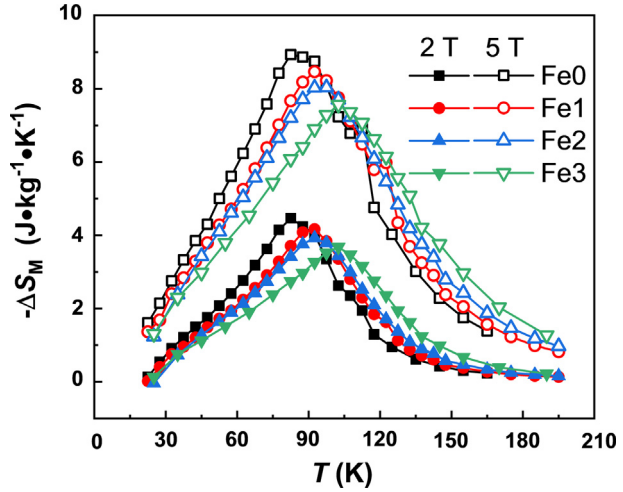

Fig. 4. Magnetic entropy changes for Fe0, Fe1, Fe2 and Fe3 microwires under $\mu_0\Delta H$ of 2 T (solid symbols) and 5 T (open symbols).

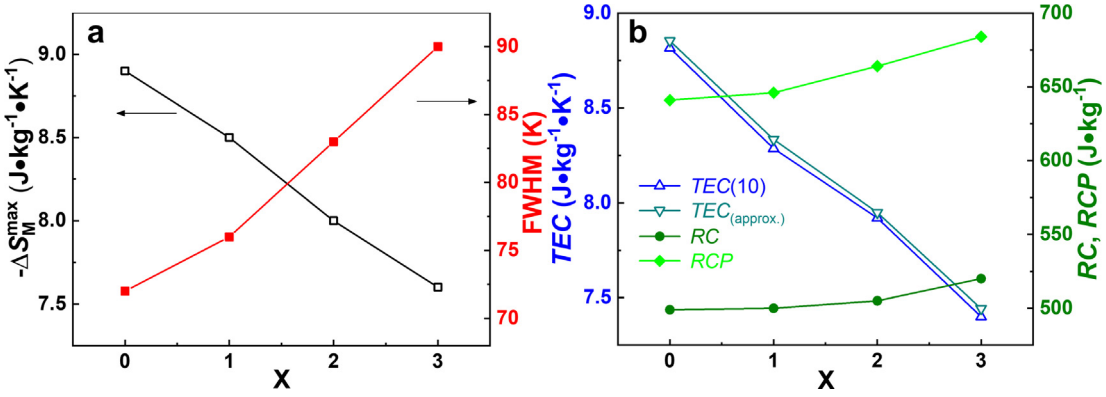

Fig. 5. The Fe content dependence of (a) $-\Delta S_M^{max}$ and FWHM, (b) *TEC*(10), $TEC_{(approx.)}$, *RC* and *RCP* for $\mu_0\Delta H$ = 5 T.

intercept of the extrapolated line and the temperature axis. The T_C of the Fe-containing GdTbCoAl microwires increases with increasing Fe content: 81, 94, 100 and 108 K for Fe0, Fe1, Fe2 and Fe3 microwires, respectively. The average increase of T_C is 9 K per Fe at.%. The increased T_C is due to the strong exchange interactions of RE-Fe and Fe-Fe pairs [39,40].

The $-\Delta S_M$ as a function of the temperature of Fe-containing GdTbCoAl microwires under $\mu_0\Delta H$ = 2 and 5 T are plotted in Fig. 4. For both field changes, $-\Delta S_M^{max}$ monotonically decreases whereas their corresponding peak temperatures increase with increasing Fe content. For $-\Delta S_M^{max}$, it decreases from 8.9 to 7.6 J kg^{-1} K^{-1} under $\mu_0\Delta H$ = 5 T for Fe0 to Fe3 as shown in Fig. 5 (a). The average reduction of $-\Delta S_M^{max}$ is 0.43 J kg^{-1} K^{-1} per Fe at.%. This small reduction in $-\Delta S_M^{max}$ with increasing Fe content is attributed to the replacement of the RE-elements with high magnetic moments by Fe.

TEC(10) is the temperature averaged $-\Delta S_M$ recently proposed by Griffith et al. [41], which refers to the maximum average of $-\Delta S_M$ over a 10 K temperature span. It is regarded as an alternative figure merit for evaluating MCE materials. It can avoid artificially large values of refrigerant capacity of MCMs in the cases of exhibiting shallow and wide peaks. *TEC*(10) can be calculated as follows [41]:

$$\mathrm{TEC}(10) = \frac{1}{10} max\left\{\int_{T_{mid}-5}^{T_{mid}+5} -S_M(T)dT\right\} \quad (2)$$

where T_{mid} is chosen by sweeping over the $-\Delta S_M(T)$ curve to obtain maximum value of *TEC*(10) at the temperature span of 10 K. In the

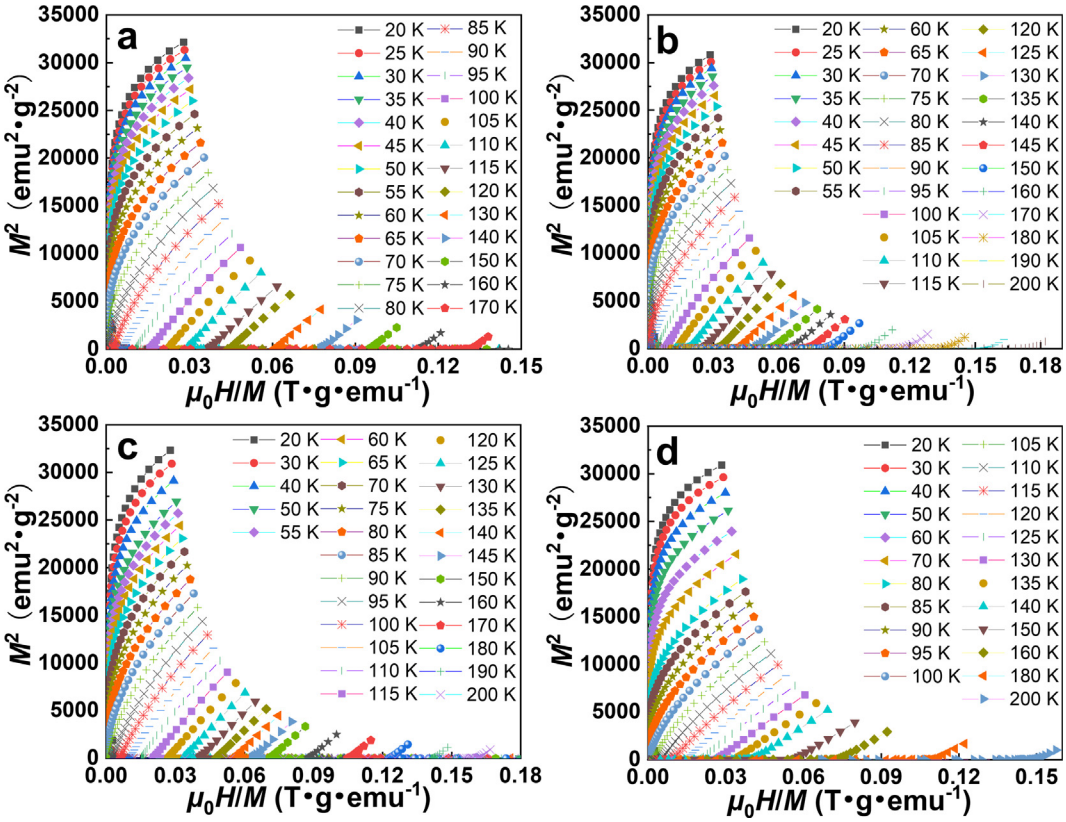

Fig. 6. Arrott plots of (a) Fe0, (b) Fe1, (c) Fe2 and (d) Fe3 microwires.

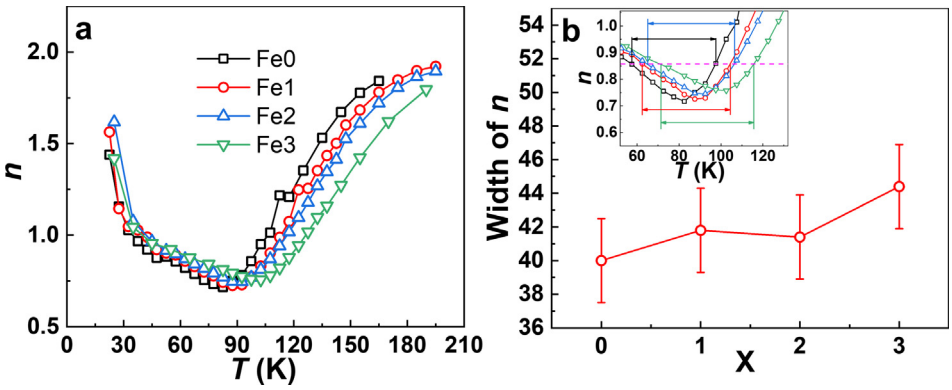

Fig. 7. (a) The temperature dependence of the exponent n. (b) Fe content dependence of the width of n, with inset showing how the width of n was obtained. Both graphs are under $\mu_0\Delta H$ = 5 T.

case that the available data for the $-\Delta S_M(T)$ curves are limited (e.g. literature data), this expression can be approximated as follows [42]:

$$TEC_{(approx.)} \approx \frac{-[\Delta S_M(T_{peak}-5)+\Delta S_M(T_{peak})+\Delta S_M(T_{peak}+5)]}{3} \quad (3)$$

The $TEC(10)$ and approximate value of $TEC(10)$, $TEC_{(approx.)}$, decrease with increasing Fe content, as shown in Fig. 5(b). The similarity of both values shows the validity of the approximation. They are in the range of $-\Delta S_M^{max}$ values, confirming the relatively broad peaks of $-\Delta S_M(T)$ curves of Fe-containing GdTbCoAl microwires.

For alloys with relatively high $-\Delta S_M^{max}$, refrigeration capacity (RC) and RCP are usually employed to evaluate cooling efficiency, and are calculated by using the following formulas [43–45]:

$$RCP = -\Delta S_M^{max} \times \delta T_{FWHM} = -\Delta S_M^{max}(T_2 - T_1) \quad (4)$$

$$RC = -\int_{T_1}^{T_2} \Delta S_M(T)dT \quad (5)$$

where T_1 and T_2 represent the endpoints of full-width at half-maximum (FWHM, i.e. working temperature range) of $-\Delta S_M(T)$ curves. Fig. 5(a) shows FWHM of $-\Delta S_M(T)$ curves. The results show that FWHM increases with increasing Fe content. Although a single material in a refrigerator device will not operate in such broad temperature span, the large $-\Delta S_M$ existing in such broad temperature range will facilitate the operation of the materials in the temperature ranges within the FWHM. The results of RCP and RC for Fe-containing GdTbCoAl microwires are shown in Fig. 5(b) for $\mu_0\Delta H$ = 5 T. RCP and RC increase with the increase of Fe content due to the enlarged FWHM of $-\Delta S_M(T)$ curves. The values of RCP and RC increase to 684 J kg^{-1} and 520 J kg^{-1}, respectively, for Fe3 microwires under $\mu_0\Delta H$ = 5 T. The increase of FWHM could be ascribed to the appearance of nanocrystals.

To determine the order of magnetic phase transition of the studied microwires, two methods were used: 1) Arrott plots (M^2 vs. H/M) and 2) the quantitative criterion based on the magnetic field dependence of MCE [46]. Fig. 6 shows the Arrott plots of all studied microwires. All the curves show positive tangent slopes for the whole measurement temperature range, indicating second-order of phase transition (SOPT) for all the studied microwires according to Banerjee's criterion [47]. For the next method, the exponent of the magnetic field dependence of MCE, represented as n, is calculated and analyzed. The relationship between $-\Delta S_M$ and $\mu_0\Delta H$ follows a power law [48]:

$$-\Delta S_M \propto \mu_0 \Delta H^n \quad (6)$$

where n is a local exponent that depends on both magnetic field and temperature. The local calculation for obtaining n is:

$$n = \frac{d\ln|\Delta S_M|}{d\ln\mu_0\Delta H} \quad (7)$$

The temperature dependence of the calculated n is shown in Fig. 7(a), which shows the typical behavior of SOPT materials in the absence of overshoot of n larger than 2. This agrees well with the observations of Fig. 6. Usually, multiple phases would appear as separated peaks in the $-\Delta S_M(T)$ curves unless the phase transition temperatures are rather close or the fractions of the additional phase are too low. In such cases, the $n(T)$ data can be used for analyzing the existence of additional phase transitions [48] where the existence of multiple phases would show additional minima in $n(T)$. This is not the case in Fig. 7(a) where no additional minimum is observed despite Fe2 and Fe3 are found with dual-phase microstructure. Fig. 7(b) presents the widths of $n(T)$ curves as a function of Fe content. The widths are obtained at n = 0.85, as shown in the inset of Fig. 7(b). The significant increase of the width is observed for the Fe3, in agreement to the widest FWHM and largest nanocrystal fraction of Fe3 microwires. The absence of additional features both in $n(T)$ and $-\Delta S_M(T)$ curves could be related to proximity of the T_C of two phases or the low fraction of nanocrystalline phase. The compositional differences between nanocrystalline phase and amorphous matrix (see Fig. S3 and

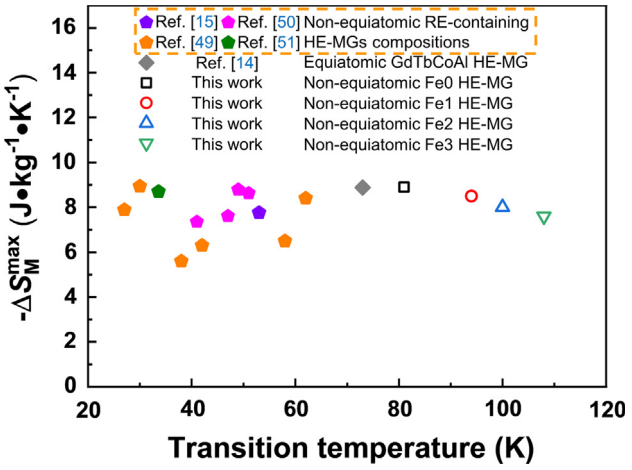

Fig. 8. MCE performance for RE-containing HE-MGs for $\mu_0\Delta H$ = 5 T. Data of the literature are collected from Refs. [14,15,49–51].

Table S1) lead to a broad T_C distribution, broadening the FWHM. The wide FWHM counteracts the small $-\Delta S_M^{max}$ reduction and therefore increases the cooling efficiency.

Fig. 8 shows the transition temperature dependence of $-\Delta S_M^{max}$ of our studied microwires in comparison with those of non-equiatomic RE-containing HE-MGs and equiatomic GdTbCoAl HE-MG. It is observed that our HE-MG alloy microwires exhibit a wide range of transition temperatures beyond the typical limit, <60 K. Furthermore, $-\Delta S_M^{max}$ is maintained in a relatively large value range as compared with those of other reported non-equiatomic RE-containing HE-MGs and equiatomic GdTbCoAl HE-MG. This demonstrates that Fe-containing GdTbCoAl HE-MG composite microwires have great application prospects as high-performance magnetic refrigerants.

4. Conclusion

With minor Fe additions, $(Gd_{36}Tb_{24}Co_{20}Al_{20})_{100-x}Fe_x$ (x = 0, 1, 2 and 3 at.%) high-entropy-alloy microwires enabled tunable Curie temperatures up to 108 K, which is beyond the typical limit of RE-containing magnetocaloric HEAs (<60 K). The T_C increases at an average rate of 9 K per Fe at.%, ascribed to the strong exchange interactions of RE-Fe and Fe-Fe pairs. Furthermore, the Fe additions facilitate the formation of amorphous/nanocrystalline dual-phase structure that leads to increased cooling efficiency, keeping relatively large $-\Delta S_M^{max}$ values (7.6–8.9 J kg^{-1} K^{-1} for 5 T) in an extended working temperature span. Compared to reported promising magnetocaloric HEAs, these microwires exhibit comparable MCE properties yet at much higher working temperatures. The large MCE performance enhanced by the appropriate compositional design and processing technique opens another direction for optimizing HEAs as high-performance MCMs.

Declaration of Competing Interest

The authors declare that they have no known competing financial interests or personal relationships that could have appeared to influence the work reported in this paper.

Acknowledgments

The authors would like to acknowledge the financial support from the National Natural Science Foundation of China under Grant Nos. 51871076, 51671070, 51801044, and 51827801, and the 66th China Postdoctoral Science Foundation under Grant No. 2019M661275. V.F. and J.L. acknowledge funding from AEI/FEDER-UE (grant PID2019-105720RB-I00), US/JUNTA/FEDER-UE (grant US-1260179), and Consejería de Economía, Conocimiento, Empresas y Universidad de la Junta de Andalucía (grant P18-RT-746). H.Y. acknowledges the fellowship from China Scholarship Council (CSC, No. 201906120183) for Visiting PhD Student program.

Appendix A. Supplementary material

Supplementary data to this article can be found online at https://doi.org/10.1016/j.matdes.2021.109824.

References

[1] T. Gottschall, K.P. Skokov, M. Fries, A. Taubel, I. Radulov, F. Scheibel, D. Benke, S. Riegg, O. Gutfleisch, Making a cool choice: the materials library of magnetic refrigeration, Adv. Energy Mater. 9 (34) (2019) 1901322, https://doi.org/10.1002/aenm.201901322.

[2] C.F. Sánchez-Valdés, P.J. Ibarra-Gaytán, J.L.S. Llamazares, M. Ávalos-Borja, P. Álvarez-Alonso, P. Gorria, J.A. Blanco, Enhanced refrigerant capacity in two-phase nanocrystalline/amorphous $NdPrFe_{17}$ melt-spun ribbons, Appl. Phys. Lett. 104 (21) (2014), https://doi.org/10.1063/1.4879544 212401.

[3] H.X. Shen, D.W. Xing, J.L. Sánchez Llamazares, C.F. Sánchez-Valdés, H. Belliveau, H. Wang, F.X. Qin, Y.F. Liu, J.F. Sun, H. Srikanth, M.H. Phan, Enhanced refrigerant capacity in Gd-Al-Co microwires with a biphase nanocrystalline/amorphous structure, Appl. Phys. Lett. 108(9) (2016) 092403, https://doi.org/10.1063/1.4943137.

[4] B.G. Shen, J.R. Sun, F.X. Hu, H.W. Zhang, Z.H. Cheng, Recent progress in exploring magnetocaloric materials, Adv. Mater. 21 (45) (2009) 4545–4564, https://doi.org/10.1002/adma.200901072.

[5] H.F. Belliveau, Y.Y. Yu, Y. Luo, F.X. Qin, H. Wang, H.X. Shen, J.F. Sun, S.C. Yu, H. Srikanth, M.H. Phan, Improving mechanical and magnetocaloric responses of amorphous melt-extracted Gd-based microwires via nanocrystallization, J. Alloys Compd. 692 (2017) 658–664, https://doi.org/10.1016/j.jallcom.2016.08.254.

[6] V.V. Khovaylo, V.V. Rodionova, S.N. Shevyrtalov, V. Novosad, Magnetocaloric effect in "reduced" dimensions: thin films, ribbons, and microwires of Heusler alloys and related compounds, Phys. Status Solidi B 251 (10) (2014) 2104–2113, https://doi.org/10.1002/pssb.201451217.

[7] D. Vuarnoz, T. Kawanami, Numerical analysis of a reciprocating active magnetic regenerator made of gadolinium wires, Appl. Therm. Eng. 37 (2012) 388–395, https://doi.org/10.1016/j.applthermaleng.2011.11.053.

[8] M.D. Kuz'min, Factors limiting the operation frequency of magnetic refrigerators, Appl. Phys. Lett. 90 (25) (2007) 251916. https://doi.org/10.1063/1.2750540.

[9] S.D. Jiang, H. Wang, D. Estevez, Y.J. Huang, L.Y. Zhang, H.X. Shen, Z.L. Ning, F.X. Qin, J.F. Sun, Surface microstructural design to improve mechanical and giant magneto-impedance properties of melt-extracted CoFe-based amorphous wires, Mater. Des. 204 (2021), https://doi.org/10.1016/j.matdes.2021.109642 109642.

[10] H. Wang, F.X. Qin, D.W. Xing, F.Y. Cao, H.X. Peng, J.F. Sun, Fabrication and characterization of nano/amorphous dual-phase FINEMET microwires, Mater. Sci. Eng, B 178 (20) (2013) 1483–1490, https://doi.org/10.1016/j.mseb.2013.09.010.

[11] B. Cantor, I.T.H. Chang, P. Knight, A.J.B. Vincent, Microstructural development in equiatomic multicomponent alloys, Mater. Sci. Eng. A 375–377 (2004) 213–218, https://doi.org/10.1016/j.msea.2003.10.257.

[12] J.W. Yeh, S.K. Chen, S.J. Lin, J.Y. Gan, T.S. Chin, T.T. Shun, C.H. Tsau, S.Y. Chang, Nanostructured high-entropy alloys with multiple principal elements: Novel alloy design concepts and outcomes, Adv. Eng. Mater. 6 (5) (2004) 299–303, https://doi.org/10.1002/adem.200300567.

[13] Y. Zhang, High-Entropy Materials, Springer, Singapore, 2019. https://doi.org/10.1007/978-981-13-8526-1.

[14] L. Xue, L.L. Shao, Q. Luo, B.L. Shen, $Gd_{25}RE_{25}Co_{25}Al_{25}$ (RE = Tb, Dy and Ho) high-entropy glassy alloys with distinct spin-glass behavior and good magnetocaloric effect, J. Alloys Compd. 790 (2019) 633–639, https://doi.org/10.1016/j.jallcom.2019.03.210.

[15] L. Liang, X. Hui, Y. Wu, G.L. Chen, Large magnetocaloric effect in $Gd_{36}Y_{20}Al_{24}Co_{20}$ bulk metallic glass, J. Alloys Compd. 457 (1–2) (2008) 541–544, https://doi.org/10.1016/j.jallcom.2007.03.101.

[16] J.T. Huo, L.S. Huo, H. Men, X.M. Wang, A. Inoue, J.Q. Wang, C.T. Chang, R.W. Li, The magnetocaloric effect of Gd-Tb-Dy-Al-M (M = Fe, Co and Ni) high-entropy bulk metallic glasses, Intermetallics 58 (2015) 31–35, https://doi.org/10.1016/j.intermet.2014.11.004.

[17] J.T. Huo, L.S. Huo, J.W. Li, H. Men, X.M. Wang, A. Inoue, C.T. Chang, J.Q. Wang, R. W. Li, High-entropy bulk metallic glasses as promising magnetic refrigerants, J. Appl. Phys. 117 (7) (2015), https://doi.org/10.1063/1.4908286 073902.

[18] J.S. Liu, G.D. Qu, X.F. Wang, H.N. Chen, Y. Zhang, G.Y. Cao, R. Liu, S.D. Jiang, H.X. Shen, J.F. Sun, Influence of Fe-doping amounts on magnetocaloric properties of Gd-based amorphous microfibers, J. Alloys Compd. 845 (2020), https://doi.org/10.1016/j.jallcom.2020.156190 156190.

[19] G.L. Liu, D.Q. Zhao, H.Y. Bai, W.H. Wang, M.X. Pan, Room temperature table-like magnetocaloric effect in amorphous $Gd_{50}Co_{45}Fe_5$ ribbon, J. Phys. D: Appl. Phys. 49 (5) (2016), https://doi.org/10.1088/0022-3727/49/5/055004 055004.

[20] L. Xue, J. Li, W.M. Yang, C.C. Yuan, B.L. Shen, Effect of Fe substitution on magnetocaloric effects and glass-forming ability in Gd-based metallic glasses, Intermetallics 93 (2018) 67–71, https://doi.org/10.1016/j.intermet.2017.11.007.

[21] A. Takeuchi, A. Inoue, Classification of bulk metallic glasses by atomic size difference, heat of mixing and period of constituent elements and its application to characterization of the main alloying element, Mater. Trans. 46 (12) (2005) 2817–2829, https://doi.org/10.2320/matertrans.46.2817.

[22] A. Inoue, Stablization of metallic supercooled liquid and bulk amorphous alloys, Acta Mater. 48 (1) (2000) 279–306, https://doi.org/10.1016/S1359-6454(99)00300-6.

[23] S. Guo, C.T. Liu, Phase stability in high entropy alloys: Formation of solid-solution phase or amorphous phase, Prog. Nat. Sci. Mater. Inter. 21 (6) (2011) 433–446, https://doi.org/10.1016/s1002-0071(12)60080-x.

[24] Y.J. Yang, B.Y. Cheng, Z.S. Jin, H.X. Gao, M.Z. Ma, X.Y. Zhang, Crystallization kinetics and mechanical properties of $Zr_{56}Cu_{24}Al_9Ni_{7-x}Ti_4Ag_x$ (x = 0, 1, 3, 5, and 7) metallic glasses, J. Alloys Compd. 816 (2020), https://doi.org/10.1016/j.jallcom.2019.152589 152589.

[25] J. Xiong, S.Q. Shi, T.Y. Zhang, A machine-learning approach to predicting and understanding the properties of amorphous metallic alloys, Mater. Des. 187 (2020), https://doi.org/10.1016/j.matdes.2019.108378 108378.

[26] Z.P. Lu, C.T. Liu, A new glass-forming ability criterion for bulk metallic glasses, Acta Mater. 50 (13) (2002) 3501–3512, https://doi.org/10.1016/s1359-6454(02)00166-0.
[27] Y. Zhang, Y.J. Zhou, J.P. Lin, G.L. Chen, P.K. Liaw, Solid-solution phase formation rules for multi-component alloys, Adv. Eng. Mater. 10 (6) (2008) 534–538, https://doi.org/10.1002/adem.200700240.
[28] D.C. Zhao, T. Yamaguchi, D. Tusbasa, W.Q. Wang, Fabrication and friction properties of the AlFeCrCo medium-entropy alloy coatings on magnesium alloy, Mater. Des. 193 (2020), https://doi.org/10.1016/j.matdes.2020.108872 108872.
[29] L.X. Shi, K.F. Yao, Composition design for Fe-based soft magnetic amorphous and nanocrystalline alloys with high Fe content, Mater. Des. 189 (2020), https://doi.org/10.1016/j.matdes.2020.108511 108511.
[30] L. Deng, A. Gebert, L. Zhang, H.Y. Chen, D.D. Gu, U. Kühn, M. Zimmermann, K. Kosiba, S. Pauly, Mechanical performance and corrosion behaviour of Zr-based bulk metallic glass produced by selective laser melting, Mater. Des. 189 (2020), https://doi.org/10.1016/j.matdes.2020.108532 108532.
[31] J. Zhou, Q.Q. Wang, X.D. Hui, Q.S. Zeng, Y.W. Xiong, K.B. Yin, B.A. Sun, L.T. Sun, M. Stoica, W.H. Wang, B.L. Shen, A novel FeNi-based bulk metallic glass with high notch toughness over 70 MPa $m^{1/2}$ combined with excellent soft magnetic properties, Mater. Des. 191 (2020), https://doi.org/10.1016/j.matdes.2020.108597 108597.
[32] R.E. Hackenberg, M.C. Gao, L. Kaufman, G.J. Shiflet, Thermodynamics and phase equilibria of the Al–Fe–Gd metallic glass-forming system, Acta Mater. 50 (9) (2002) 2245–2258, https://doi.org/10.1016/s1359-6454(01)00435-9.
[33] Z.P. Lu, J. Shen, D.W. Xing, J.F. Sun, C.T. Liu, Binary eutectic clusters and glass formation in ideal glass-forming liquids, Appl. Phys. Lett. 89 (7) (2006), https://doi.org/10.1063/1.2336597 071910.
[34] B.C. Wei, W. Löser, L. Xia, S. Roth, M.X. Pan, W.H. Wang, J. Eckert, Anomalous thermal stability of Nd–Fe–Co–Al bulk metallic glass, Acta Mater. 50 (17) (2002) 4357–4367, https://doi.org/10.1016/s1359-6454(02)00272-0.
[35] C.J. Chen, K.K. Wong, R.P. Krishnan, L. Zhi Feng, D.H. Yu, Z.P. Lu, S.M. Chathoth, Highly collective atomic transport mechanism in high-entropy glass-forming metallic liquids, J. Mater. Sci. Technol. 35 (1) (2019) 44–47, https://doi.org/10.1016/j.jmst.2018.09.008.
[36] A. Inoue, A. Takeuchi, T. Zhang, Ferromagnetic bulk amorphous alloys, Metall. Mater. Trans. A 29 (7) (1998) 1779–1793, https://doi.org/10.1007/s11661-998-0001-9.
[37] W.H. Wang, Roles of minor additions in formation and properties of bulk metallic glasses, Prog. Mater. Sci. 52 (4) (2007) 540–596, https://doi.org/10.1016/j.pmatsci.2006.07.003.
[38] Y.T. Wang, Z.Y. Pang, R.J. Wang, D.Q. Zhao, M.X. Pan, B.S. Han, W.L. Wang, W.H. Wang, Doping-induced formation of bulk nanocrystalline alloy from metallic glass with controllable microstructure and properties, J. Non-Cryst. Solids 352 (5) (2006) 444–449, https://doi.org/10.1016/j.jnoncrysol.2006.01.015.
[39] Z.G. Zheng, X.C. Zhong, K.P. Su, H. Yu, Z.W. Liu, D.C. Zeng, Magnetic properties and large magnetocaloric effects in amorphous Gd-Al-Fe alloys for magnetic refrigeration, Sci. China Phys. Mech. Astron. 54 (7) (2011) 1267–1270, https://doi.org/10.1007/s11433-011-4363-4.
[40] P. Hansen, C. Clausen, G. Much, M. Rosenkranz, K. Witter, Magnetic and magneto-optical properties of rare-earth transition-metal alloys containing Gd, Tb, Fe, Co, J. Appl. Phys. 66 (2) (1989) 756–767, https://doi.org/10.1063/1.343551.
[41] L.D. Griffith, Y. Mudryk, J. Slaughter, V.K. Pecharsky, Material-based figure of merit for caloric materials, J. Appl. Phys. 123 (3) (2018), https://doi.org/10.1063/1.5004173 034902.
[42] Law J.Y., Franco V., Magnetocaloric Composite Materials, Encyclopedia of Materials: Composites. https://doi.org/10.1016/B978-0-12-819724-0.00038-0.
[43] M.F. Qian, X.X. Zhang, Z.G. Jia, X.H. Wan, L. Geng, Enhanced magnetic refrigeration capacity in Ni-Mn-Ga micro-particles, Mater. Des. 148 (2018) 115–123, https://doi.org/10.1016/j.matdes.2018.03.062.
[44] M.F. Qian, X.X. Zhang, X. Li, R.C. Zhang, P.G. Martin, J.F. Sun, L. Geng, T.B. Scott, H.X. Peng, Magnetocaloric effect in bamboo-grained Ni-Mn-Ga microwires over a wide working temperature interval, Mater. Des. 190 (2020), https://doi.org/10.1016/j.matdes.2020.108557 108557.
[45] S.K. Pal, C. Frommen, S. Kumar, B.C. Hauback, H. Fjellvåg, G. Helgesen, Enhancing giant magnetocaloric effect near room temperature by inducing magnetostructural coupling in Cu-doped MnCoGe, Mater. Des. 195 (2020), https://doi.org/10.1016/j.matdes.2020.109036 109036.
[46] J.Y. Law, V. Franco, L.M. Moreno-Ramirez, A. Conde, D.Y. Karpenkov, I. Radulov, K.P. Skokov, O. Gutfleisch, A quantitative criterion for determining the order of magnetic phase transitions using the magnetocaloric effect, Nat. Commun. 9 (1) (2018) 2680, https://doi.org/10.1038/s41467-018-05111-w.
[47] B.K. Banerjee, On a generalised approach to first and second order magnetic transitions, Phys. Lett. 12 (1) (1964) 16–17, https://doi.org/10.1016/0031-9163(64)91158-8.
[48] V. Franco, A. Conde, V.K. Pecharsky, K.A. Gschneidner Jr., Field dependence of the magnetocaloric effect in Gd and $(Er_{1-x}Dy_x)Al_2$: does a universal curve exist?, EPL 79 (4) (2007) 47009, https://doi.org/10.1209/0295-5075/79/47009.
[49] Q. Luo, B. Schwarz, N. Mattern, J. Eckert, Giant irreversible positive to large reversible negative magnetic entropy change evolution in Tb-based bulk metallic glass, Phys. Rev. B 82 (2) (2010), https://doi.org/10.1103/PhysRevB.82.024204 024204.
[50] C.M. Pang, C.C. Yuan, L. Chen, H. Xu, K. Guo, J.C. He, Y. Li, M.S. Wei, X.M. Wang, J.T. Huo, B.L. Shen, Effect of Yttrium addition on magnetocaloric properties of Gd-Co-Al-Ho high entropy metallic glasses, J. Non-Cryst. Solids 549 (2020), https://doi.org/10.1016/j.jnoncrysol.2020.120354 120354.
[51] Z.Q. Dong, Z.J. Wang, S.H. Yin, Magnetic properties and magneto-caloric effect (MCE) in $Cu_{22}Al_{18}Ho_{22}Tm_{20}Gd_{18}$ amorphous ribbons, J. Magn. Magn. Mater. 514 (2020), https://doi.org/10.1016/j.jmmm.2020.167270 167270.